



Inelastic neutron scattering in the weakly coupled triangular spin tube candidate CsCrF₄Hodaka Kikuchi  and Shinichiro Asai*Institute for Solid State Physics, University of Tokyo, Kashiwa, Chiba 277-8581, Japan*Hirotaka Manaka *Graduate School of Science and Engineering, Kagoshima University, Korimoto, Kagoshima 890-0065, Japan*Masato Hagihala and Shinichi Itoh *Neutron Science Division, Institute of Materials Structure Science, High Energy Accelerator Research Organization, Tsukuba, Ibaraki 305-0801, Japan*Takatsugu Masuda *Institute for Solid State Physics, University of Tokyo, Kashiwa, Chiba 277-8581, Japan;
Institute of Materials Structure Science, High Energy Accelerator Research Organization, Ibaraki 305-0801, Japan;
and Trans-scale Quantum Science Institute, The University of Tokyo, Tokyo 113-0033, Japan*

(Received 29 December 2022; revised 28 February 2023; accepted 14 April 2023; published 3 May 2023)

We performed inelastic neutron scattering (INS) experiments to measure spin dynamics in a polycrystalline sample of the spin tube candidate CsCrF₄. The compound exhibits a successive phase transition from a paramagnetic phase through an intermediate-temperature (IT) phase of a 120° structure to a low-temperature (LT) phase of another 120° structure. An elaborate comparison of observed and calculated neutron spectra in the LT phase reveals that the spin Hamiltonian is identified as antiferromagnetic spin tubes including perturbative terms of intertube interaction, Dzyaloshinskii-Moriya interaction, and single-ion anisotropy. A phase diagram for the ground state is classically calculated. A set of parameters in the spin Hamiltonian obtained from the INS spectra measured in the LT phase is quite close to the boundary of the phase of the 120° structure of the IT phase. The INS spectra measured in the IT phase are, surprisingly, the same as those in the LT phase on the level of powder-averaged spectra, even though the magnetic structures in the IT and LT phases are different. Identical dynamical structures compatible with two different static structures are observed. No difference in the observed spectra indicates no change in the spin Hamiltonian with the temperature, suggesting that the origin of the successive phase transition is a spin-entropy-driven mechanism in the spin system located near the phase boundary.

DOI: [10.1103/PhysRevB.107.184405](https://doi.org/10.1103/PhysRevB.107.184405)**I. INTRODUCTION**

Geometrically frustrated magnets have attracted great interest because of the nontrivial magnetic states induced at low temperatures. The magnetic states of lattices, including the triangular basic unit, are incompatible with Néel order, and they are macroscopically degenerate [1]. An example of a one-dimensional frustrated system is a triangular spin tube in which antiferromagnetic spins on triangles are arrayed in one dimension, which has been theoretically studied extensively. In a regular triangular spin tube with Heisenberg spin, the ground state is the dimerized nonmagnetic state with the units of the two-site rung singlet [2]. The spin correlation exponentially decays, and the excited state is separated by a finite spin gap [3–8]. In an asymmetric triangular spin tube in which Z_2 symmetry is broken, the spin gap is suppressed, and a Tomonaga-Luttinger liquid with vector chiral order is predicted [9,10]. In contrast to the accumulative theoretical studies, experimental study has been limited to an $S = 3/2$ spin tube candidate, CsCrF₄ [11–16], for lack of a model material.

In a real compound, exchange interactions between triangular spin tubes are not negligible, and hence, the geometry of the interactions between the tubes is important for determination of the ground state. An example of the geometry is shown in Fig. 1(a), where the regular triangles form a two-dimensional triangular lattice. The lattice is equivalent to a kagome lattice with second-neighbor interaction, which is called the kagome-triangular (KT) lattice, as shown in Fig. 1(b). The ground state of a Heisenberg classical kagome antiferromagnet is a magnetically ordered state, a 120° structure with macroscopic degeneracy which is vulnerable to fluctuation. Coplanar 120° structures with large entropy, in which spins are confined in a plane, are selected at finite temperatures using the order by disorder mechanism [17–19]. Experimentally, various types of 120° structures with $Q = 0$ have been reported: A structure with positive chirality selected by Dzyaloshinskii-Moriya interaction in Fe and Cr jarosite [20–24], one with negative chirality in the semimetals Mn₃Sn and Mn₃Ge [25], and a tail-chase structure selected by magnetic dipole interaction in Mn²⁺ fluoride [26,27]. The

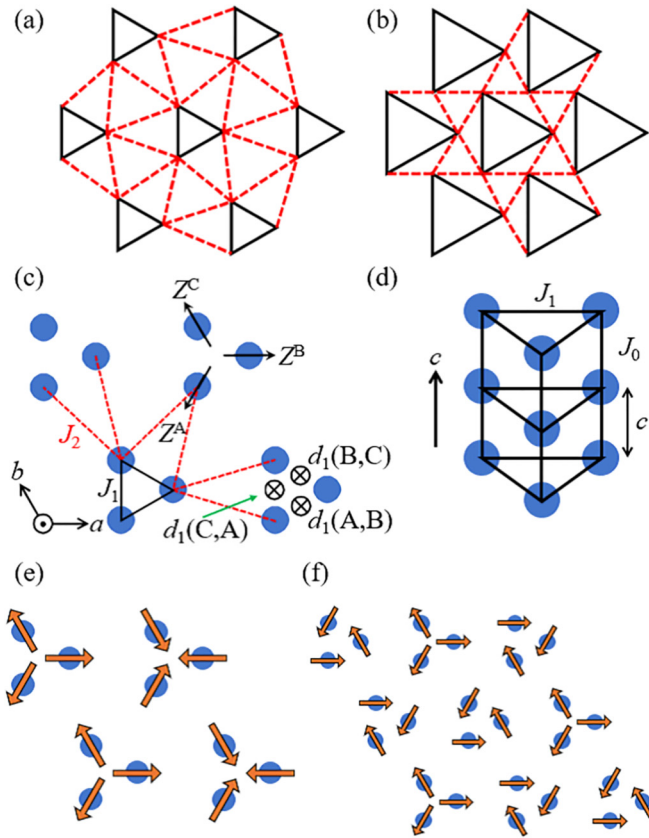


FIG. 1. (a) An example of the geometry of coupled spin tubes viewed from the tube direction. (b) Schematic description of the kagome-triangular lattice. (c) Crystal structure of CsCrF₄ projected in the crystallographic *ab* plane. Blue circles indicate the Cr³⁺ ion. Z^α ($\alpha = A, B, C$) is the *Z* axis locally defined on the α site of the Cr³⁺ ion, and $d_1(\alpha, \beta)$ ($\alpha, \beta = A, B, C$) is the DM vector. (d) Perspective view of the spin tube of CsCrF₄. (e) Magnetic structure of CsCrF₄ in the IT phase. (f) Magnetic structure of CsCrF₄ in the LT phase, which is used for linear spin-wave calculations in the present paper.

introduction of a second-neighbor ferromagnetic interaction in a Heisenberg KT lattice leads to a cuboc structure, a non-coplanar multi-*Q* structure with 12 sublattices with the spins directed along the 12 middle points of a cube, and the introduction of a second-neighbor antiferromagnetic interaction leads to a $\sqrt{3} \times \sqrt{3}$ structure [28–30].

CsCrF₄ is a candidate for the triangular spin tube in which intertube and rung couplings form a KT lattice [11–16]. The crystal structure of CsCrF₄, where Cr³⁺ ions carrying spin $S = 3/2$ are displayed and Cs⁺ and F[−] ions are omitted, is shown in Figs. 1(c) and 1(d). As speculated from the bond lengths, exchange interactions along the leg, J_0 , and the rung, J_1 , in the spin tube would be dominant, and one between the spin tubes, J_2 , would be weak. The Cr³⁺ network in the *ab* plane shown in Fig. 1(a) is equivalent to the KT lattice in Fig. 1(b), where the nearest-neighbor kagome interaction corresponds to J_2 , and the second-neighbor one corresponds to J_1 . The magnetic susceptibility of this compound has a broad maximum at $T \simeq 60$ K, and hysteresis is observed below $T = 4$ K [11]. Neutron diffraction scattering experiments probed a successive phase transition with the critical

temperatures $T_{N1} = 2.8$ K and $T_{N2} = 3.5$ K [15]. The magnetic structure for the low-temperature (LT) phase at $T \leq T_{N1}$ is a 120° structure with $\mathbf{q}_m = (1/2, 0, 1/2)$, as shown in Fig. 1(e), where \mathbf{q}_m is a propagation vector. The one for the intermediate-temperature (IT) phase at $T_{N1} \leq T \leq T_{N2}$ used for the spin-wave calculation in the present paper is a 120° structure with $\mathbf{q}_m = (1/3, 1/3, 1/2)$, as shown in Fig. 1(f). The correlation length was reported to be 100–200 Å [15]. The structure of the LT phase is different from the theoretical prediction of cuboc or $\sqrt{3} \times \sqrt{3}$ structure in the Heisenberg KT lattice [28–30]. It was proposed that small perturbations, including intertube interaction, Dzyaloshinskii-Moriya (DM) interaction, and single-ion anisotropy, select the observed magnetic structure in the LT phase. Nevertheless, the spin Hamiltonian has not been identified yet.

In this study, we perform inelastic neutron scattering (INS) experiments to measure the spin dynamics of a polycrystalline sample of CsCrF₄. The spin Hamiltonian is identified as weakly coupled antiferromagnetic spin tubes using KT geometry. An intertube interaction, single-ion anisotropy, and DM interaction play an important role in the selection of the ground state. The set of parameters in the spin Hamiltonian suggests that the compound is located in the phase of $\mathbf{q}_m = (1/2, 0, 1/2)$ and is close to the boundary of the phase of $\mathbf{q}_m = (1/3, 1/3, 1/2)$. The spectra in both IT and LT phases are measured, and they are qualitatively the same. Identical dynamical structures compatible with different static structures are observed. A spin-entropy-driven mechanism is suggested for the origin of the successive phase transition.

II. EXPERIMENTAL DETAILS

To collect INS spectra in a wide momentum *Q*-energy $\hbar\omega$ space, INS experiments were carried out using the High Resolution Chopper (HRC) spectrometer [31] installed at BL12 at Japan Proton Accelerator Research Complex / Materials and Life Science Experimental Facility (J-PARC/MLF). A polycrystalline sample of CsCrF₄ with a mass of 5.07 g prepared with a solid-state reaction method was used [11,12]. The frequency of the Fermi chopper was 100 Hz. Neutrons with incident energies E_i of 3.05 and 15.3 meV, which were simultaneously selected using the repetition-rate multiplication technique, were used. A ³He cryostat was used to achieve low temperatures. The data reduction was performed using the HANA software [32]. After first lowering the temperature to 0.8 K, INS spectra were measured at increasing temperatures.

To measure the temperature dependence of low-energy excitation, INS experiments were carried out using the high-energy resolution cold neutron triple-axis spectrometer (HER) installed at the C11 beam port at Japan Research Reactor No. 3 (JRR-3). A polycrystalline sample with a mass of 2.69 g was used. An orange-type cryostat was used. The collimator setup was guide-open-radial collimator-open. A Be/pyrolytic graphite (PG) filter for elimination of the second-order harmonics of neutrons, which automatically switches at $E_i = 5$ meV, was set in front of the sample. A Be filter was used for $E_i \leq 5$ meV. A tunable PG filter [33,34] was used for $E_i > 5$ meV. The final neutron energy was fixed at $E_f = 3.64$ meV. The temperature

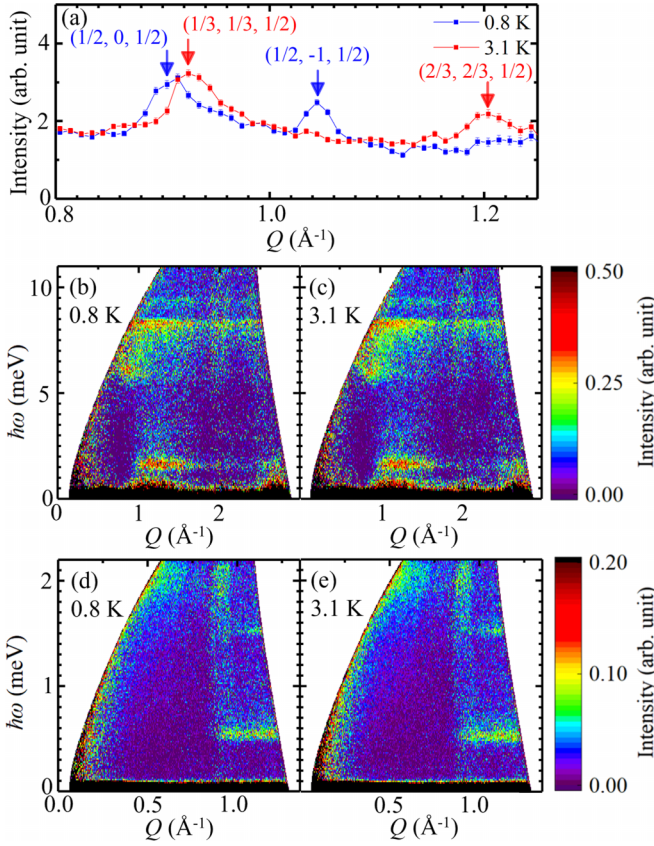


FIG. 2. INS spectra measured by the HRC spectrometer. (a) Elastic part of INS spectra measured at $E_i = 3.05$ meV, where the integration range is $-0.15 \leq \hbar\omega \leq 0.15$ meV. Blue and red symbols indicate 0.8 and 3.1 K, respectively. INS spectra measured with $E_i = 15.3$ meV at (b) 0.8 K and (c) 3.1 K. INS spectra measured with $E_i = 3.05$ meV at (d) 0.8 K and (e) 3.1 K.

dependence of INS spectra was measured under increasing temperature.

III. EXPERIMENTAL RESULTS

The elastic part of the measured INS spectra with $E_i = 3.05$ meV at 0.8 K in the LT phase and at 3.1 K in the IT phase using the HRC spectrometer is shown in Fig. 2(a). Magnetic peaks with $\mathbf{q}_m = (1/2, 0, 1/2)$ are observed at 0.8 K, and peaks with $\mathbf{q}_m = (1/3, 1/3, 1/2)$ are observed at 3.1 K. The absence of a peak with $\mathbf{q}_m = (1/2, -1, 1/2)$ at 1.04 \AA^{-1} at 3.1 K means the absence of the coexistence of IT and LT phases at 3.1 K. The absence of a peak with $\mathbf{q}_m = (2/3, 2/3, 1/2)$ at 1.19 \AA^{-1} at 0.8 K means the absence of coexistence at 0.8 K as well. These results are consistent with previous neutron diffraction measurements [15].

Figures 2(b) and 2(d) show INS spectra in the LT phase measured at $E_i = 15.3$ and 3.05 meV, respectively. Magnetic excitations up to 10 meV are observed, with flat intensities at 0.5 and 1.5 meV and a continuous intensity at 6–8 meV. The flat intensities modulate with a periodicity of about 1.6 \AA^{-1} , which coincides with the reciprocal lattice constant in the c^* direction. This fact implies that the system is quasi-one-dimensional with strong interaction in the c direc-

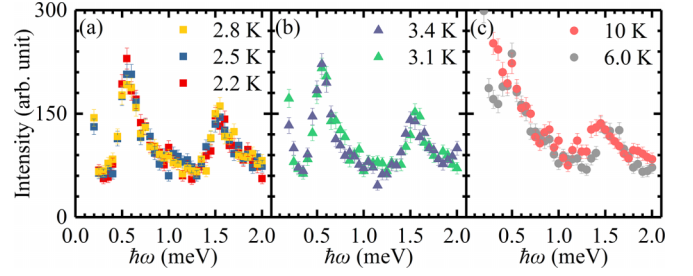


FIG. 3. Constant Q scans at $Q = 1.05 \text{ \AA}^{-1}$ collected in (a) the LT phase, (b) the IT phase, and (c) the paramagnetic phase measured by the HER spectrometer.

tion. Furthermore, the absence of intensity at Q smaller than 0.8 \AA^{-1} , which corresponds to $c^*/2$, indicates that the main interaction is antiferromagnetic rather than ferromagnetic. Note that Cr-Cr spacing along the c axis is the lattice constant c , as shown in Fig. 1(d). Figures 2(c) and 2(e) show INS spectra in the IT phase measured at $E_i = 15.3$ and 3.05 meV, respectively. Surprisingly, no qualitative difference is found in the energy range of $\hbar\omega \gtrsim 0.1$ meV between the spectra in the LT and IT phases, even though diffraction profiles sliced from the same data set exhibit magnet peaks with different propagation vectors and the absence of phase coexistence, as shown in Fig. 2(a).

The temperature dependence of constant- Q scans measured at $Q = 1.05 \text{ \AA}^{-1}$ using the HER spectrometer is shown in Figs. 3(a)–3(c). The squares, triangles, and circles indicate data in the LT, IT, and paramagnetic phases, respectively. Well-defined excitations are observed at 0.5 and 1.5 meV in both the LT and IT phases, and the spectra are qualitatively the same. The results are consistent with those measured using the HRC spectrometer. At $T = 6$ K, which is higher than T_{N2} , the inelastic excitations at 0.5 and 1.5 meV are still observed. At $T = 10$ K, paramagnetic excitation is enhanced, and the peaks are smeared.

IV. ANALYSIS

The INS cross section of CsCrF_4 was calculated based on linear spin-wave theory using the SPINW package [35]. An analytic approximation was adopted for the magnetic form factor of the Cr^{3+} ions [36]. The following Hamiltonian was used according to a previous study [15]:

$$\begin{aligned} \mathcal{H} = & \sum_{\mathbf{l}_\alpha, \mathbf{l}_\beta, \mathbf{l}'_\beta} \{ J_0 \mathbf{S}(\mathbf{l}_\alpha) \cdot \mathbf{S}(\mathbf{l}_\alpha + \mathbf{c}) + J_1 \mathbf{S}(\mathbf{l}_\alpha) \cdot \mathbf{S}(\mathbf{l}_\beta) \\ & + J_2 \mathbf{S}(\mathbf{l}_\alpha) \cdot \mathbf{S}(\mathbf{l}'_\beta) + \mathbf{d}_{1(\alpha,\beta)} \cdot \mathbf{S}(\mathbf{l}_\alpha) \times \mathbf{S}(\mathbf{l}_\beta) \\ & + D(S^{Z^\alpha}(\mathbf{l}_\alpha))^2 \}, \end{aligned} \quad (1)$$

where J_0 and J_1 are the leg and rung interactions in the spin tube in Fig. 1(d) and J_2 is an intertube interaction in Fig. 1(c). $\mathbf{d}_{1(\alpha,\beta)}$ is DM vectors between the α and β sites of Cr^{3+} ions in the triangle, D is single-ion anisotropy, and Z^α is the local Z axis defined at the α site, as shown in Fig. 1. \mathbf{l}_α is the position vector of the α site in lattice \mathbf{l} , and \mathbf{c} is the unit vector of the crystal lattice along the c axis. The sum is taken for \mathbf{l}_α , \mathbf{l}_β , and \mathbf{l}'_β over the entire crystal, where $\alpha \neq \beta$ and $\mathbf{l} \neq \mathbf{l}'$.

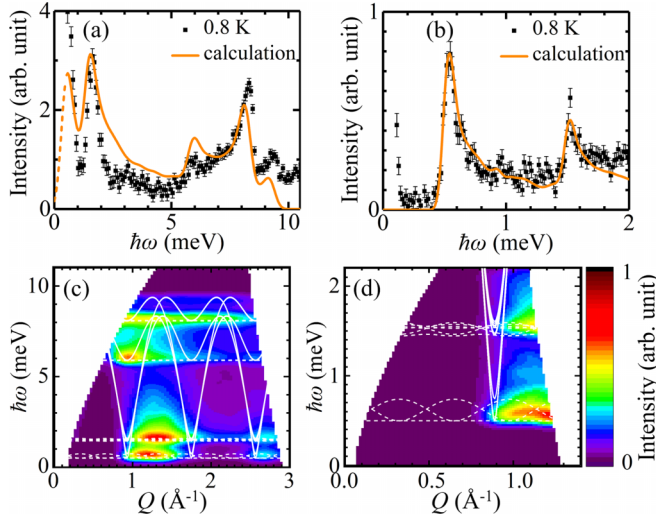


FIG. 4. One-dimensional cuts of measured and calculated INS spectra in (a) wide and (b) narrow energy ranges. Symbols and solid curves indicate experiment and calculation, respectively. INS spectra calculated by linear spin-wave theory in (c) wide and (d) narrow energy ranges. The white solid and dashed curves in (c) are dispersion curves calculated on a single crystal in the c^* and a^* directions, respectively.

The magnetic structure shown in Fig. 1(e) is used for the calculation in the LT phase.

One-dimensional (1D) cuts of measured and calculated INS spectra are shown in Figs. 4(a) and 4(b) for wide and narrow energy ranges, respectively. The measured spectrum in the former is cut from Fig. 2(b) with the integration range of $1.2 \leq Q \leq 1.5 \text{ \AA}^{-1}$, and that in the latter is cut from Fig. 2(d) with the range of $1.0 \leq Q \leq 1.1 \text{ \AA}^{-1}$. Parameters J_0 , J_1 , $d_{1(\alpha,\beta)}$, and D were determined so that the peak energies of the calculation reproduce those of the experiment. Errors were determined by the intervals of the parameters in the search. The obtained parameters are summarized in Table I. The digits in parentheses are the errors. The estimate of J_2 will be explained later. The calculated spectra for the polycrystalline sample using Eq. (1) and parameters in Table I are shown in Figs. 4(c) and 4(d) for wide and narrow energy ranges, respectively. The instrumental resolutions for Q and $\hbar\omega$ are convoluted in Figs. 4(c) and 4(d). The calculation reasonably reproduces the measured spectra in Figs. 2(b) and 2(d). Since the leg (J_0) and rung (J_1) interactions are dominant and the intertube (J_2) one is small, the spin Hamiltonian is identified as antiferromagnetic spin tubes which are weakly coupled by KT geometry. The white solid and dashed curves in Fig. 4(c) show the dispersion curves of the single crystal in the c^* and

TABLE I. Parameters of the spin Hamiltonian. J_0 , J_1 , d_1 , and D are determined by the comparison between calculation and experiment in the LT phase. J_2 is determined from the lower limit of J_2 estimated by the instrumental energy resolution (see text).

J_0 (meV)	J_1 (meV)	J_2 (μeV)	d_1 (μeV)	D (μeV)
2.35 (5)	1.00 (5)	-4(3)	-47(2)	-4.6(2)

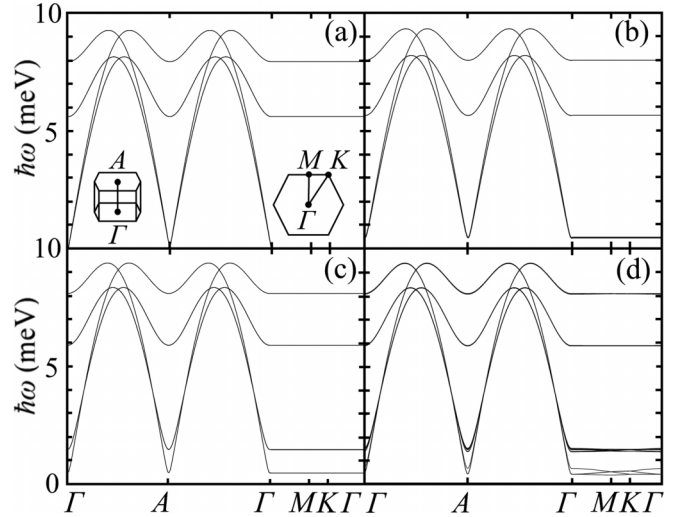


FIG. 5. Dispersion curves of a single-crystalline sample of CsCrF₄ calculated with four sets of spin parameters described in Table II: (a) case 1, (b) case 2, (c) case 3, and (d) case 4.

a^* directions, respectively. The energies of the flat intensities at 0.5, 1.5, 6.0, and 8.0 meV in the polycrystalline spectrum are identical to the dispersion curves of the single crystal in the a^* direction. They are almost independent of Q because of small J_2 . The Q dependence is rather enhanced at 0.5 meV, but it is not detected experimentally. The instrumental resolution was thus used to estimate the lower limit of J_2 (<0), where J_2 was taken to be ferromagnetic to ensure the spin structure reported previously [15]. The lower limit, which is the maximum of the absolute value in this case, was estimated to be $-7 \mu\text{eV}$. The round off of half of the lower limit, $-4 \mu\text{eV}$, was determined to be J_2 . By comparing the polycrystalline and single-crystalline spectra, it is found that well-defined flat intensities in an INS polycrystalline spectrum are ascribed to the one-dimensionality of a spin system. In contrast, the dispersion in the c^* direction induces the intensity spread in a wide Q - $\hbar\omega$ range. The ratio of J_0 and J_1 was reported to be about 1/2 in a first-principles calculation [37]. The ratios estimated in the present experiment are in good agreement with the calculation.

V. DISCUSSION

To understand the influence of each parameter in the spin Hamiltonian on the INS spectrum, dispersion curves among reciprocal lattice points with high symmetry are calculated in Figs. 5(a)–5(d) for four cases, where the parameters are shown in Table II. In case 1, which corresponds to an isolated spin

TABLE II. Parameters of the spin Hamiltonian for dispersion curves of the single-crystalline sample used in Figs. 5(a)–5(d).

	J_0 (meV)	J_1 (meV)	J_2 (μeV)	d_1 (μeV)	D (μeV)
Case 1	2.35	1.00	0	0	0
Case 2	2.35	1.00	0	0	-4.6
Case 3	2.35	1.00	0	-47	-4.6
Case 4	2.35	1.00	-4	-47	-4.6

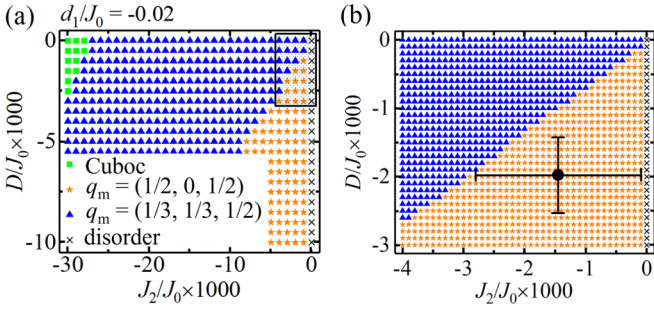


FIG. 6. Phase diagram of CsCrF₄ calculated using the Luttinger-Tisza method. (a) The D - J_2 phase diagram with $J_0 = 1$, $J_1 = 0.43$, and $d_1 = -0.02$. (b) Enlarged phase diagram of the region surrounded by the solid rectangle in (a).

tube, the excitation is dispersive along the c^* axis (from Γ to A) and dispersionless perpendicular to the c^* axis (from Γ through K to M). Periodicity along the c^* axis is half of the crystal lattice because of the antiferromagnetic leg interaction J_0 . Our analysis suggests that two modes appear at energies of $\sqrt{27J_0J_1/2}$ and $\sqrt{27J_0J_1}$ at the Γ and A points. This means that the dispersive modes in the high-energy region of $5.5 \leq \hbar\omega \leq 9$ meV are from the rung interaction J_1 .

In case 2, as shown in Fig. 5(b), single-ion anisotropy D breaks the rotational symmetry in the ab plane, lifts the degeneracy of the ground state, and induces an energy gap of 0.5 meV at $(h, k, 1/2)$, including the Γ , A , K , and M points. In case 3, as shown in Fig. 5(c), the DM interaction d_1 lifts the first excited state, and another mode appears at 1.5 meV. In case 4, as shown in Fig. 5(d), the intertube interaction J_2 makes the flat mode dispersive in the ab plane. The dispersion is larger at lower energies but still within the energy resolution. The results indicate that the effect of intertube interaction is negligibly small in CsCrF₄ even though it is important for the determination of the ground state. The dynamics of this compound is thus dominated by the isotropic spin tube, and the effect of small perturbations is detected as the energy gaps at the low energies.

In a coplanar 120° structure in a kagome lattice, certain spins surrounded by spins pointing in the same direction, such as the six spins of a hexagon or spins on a certain line, can be locally tilted from the plane without an energy cost, i.e., while keeping the angle among the adjacent spins at 120° . Such a mode is called a zero-energy mode [38,39]. The mode is lifted by DM and/or dipole interactions, and it is experimentally observed as flat excitations [27,39–41]. The flat mode in CsCrF₄ is, however, different from the zero-energy mode because it appears as the result of the lift of the degeneracy of the ground state in the quasi-isolated triangular spin system by the single-ion anisotropy and DM interaction.

A classical phase diagram of the ground state using the Luttinger-Tisza method [42,43] was calculated using Eq. (1), as shown in Fig. 6(a), where J_0 was set to 1. The cuboc structure, a 120° structure with $\mathbf{q}_m = (1/2, 0, 1/2)$, and the $\sqrt{3} \times \sqrt{3}$ structure, with $\mathbf{q}_m = (1/3, 1/3, 1/2)$, exist. The disordered state of isolated spin tubes at $J_2 = 0$ is indicated by crosses. The region surrounded by the solid rectangle in Fig. 6(a) is enlarged in Fig. 6(b). The solid circle is the posi-

tion of the parameters obtained in the present study. CsCrF₄ locates in the phase of $\mathbf{q}_m = (1/2, 0, 1/2)$, which is consistent with the magnetic structure in the LT phase [15]. It is quite close to the phase boundary for the $\mathbf{q}_m = (1/3, 1/3, 1/2)$ phase.

Let us discuss the origin of the successive phase transition. The IT phase with $\mathbf{q}_m = (1/3, 1/3, 1/2)$ structure is stable if a small lattice distortion suppresses D or enhances J_2 with the increase of the temperature. The INS spectra in the IT and LT phases were, however, the same, and the change in the parameters cannot be the origin. For confirmation, we calculated the INS spectra of the IT phase using parameters located in the phase of $\mathbf{q}_m = (1/3, 1/3, 1/2)$ near the boundary to the phase of $\mathbf{q}_m = (1/2, 0, 1/2)$. The calculated spectra were totally different from the observed one; a small change in the parameters made a drastic change in the spectrum no matter how small the change was, which is described in the Appendix. Therefore, the origin of the successive transition in CsCrF₄ is not a change in the parameters of the spin Hamiltonian due to a change in the lattice with temperature. The spin Hamiltonian remains the same in the measured temperature range. Given that the set of parameters is close to the phase boundary between the two magnetic structures, the internal energies are close to one another. In this situation, the magnetic structure with larger internal energy in the IT phase can be selected by thermal fluctuation if the spin entropy is large. The origin of the successive phase transition is thus suggested to be a spin-entropy-driven mechanism in the spin system located near the phase boundary.

There are few previous studies on the comparison of INS spectra in the IT and LT phases in spite of the existence of numerous compounds which undergo a successive phase transition: LiNiPO₄ [44] and Li₂NiW₂O₈ [45], which change from a commensurate structure in the IT phase to an incommensurate structure in the LT phase; CsCoCl₃ [46] and CuFeO₂ [47,48], which change from partial order to full order; and CsMnI₃ [49], which changes from a collinear to 120° structure while keeping the propagation vector the same. Among them, CsMnI₃ is the only compound for which spectra in both the IT and LT phases have been measured. The spectra, including dispersion curves and intensities, in the IT and LT phases are clearly different, even though the propagation vectors are identical. In contrast, in CsCrF₄, the spectra in the IT and LT phases are approximately identical in terms of the level of powder-averaged data, while the propagation vectors are different. In addition, the correlation length in the IT phase was reported to be 100–200 Å, in contrast to the long-range correlation in the LT phase [15]. Of course, the detailed structures of the spectra in the a^*-b^* plane in IT and LT phases, which can be observed using a combination of a single crystal and a perfect spectrometer, would differ from one another. The present study demonstrates that dynamical structures in different phases can be very similar, even though the static structures differ in a compound exhibiting successive transition.

The ground state of a spin $S = 3/2$ triangular spin tube is a valence bond solid state with dimerization, and an energy gap opens between the ground and excited states [7]. Such a gap has been observed in spin gap systems, including the spin $S = 1$ Haldane chain, spin $S = 1/2$ spin-Peierls system,

and spin ladder, with INS experiments. The spin gap has even been observed in compounds with a magnetically ordered state induced by interchain interaction or impurities, such as the Haldane chain CsNiCl_3 [50], impurity-doped spin-Peierls compound CuGeO_3 [51], and impurity-doped Haldane chain $\text{PbNi}_2\text{V}_2\text{O}_8$ [52,53]. In the case of the spin $S = 3/2$ spin tube compound CsCrF_4 in the present study, the gap is estimated to be about 0.006 meV ($=0.0025J_{\text{leg}}$) [7]. This is much smaller than the instrumental resolution, and it was not observed in the present study.

VI. SUMMARY

In summary, the spin Hamiltonian of CsCrF_4 was identified as weakly coupled antiferromagnetic spin tubes through INS experiments. The set of parameters obtained from the experiment in the LT phase was quite close to the phase boundary between the 120° structure with $\mathbf{q}_m = (1/2, 0, 1/2)$ and the one with $\mathbf{q}_m = (1/3, 1/3, 1/2)$. The observed INS spectra in the IT and LT phases were qualitatively the same even though the magnetic structures were different. The origin of the successive phase transition turned out to be a spin-entropy-driven mechanism. The observation of identical dynamical structures compatible with different static structures in the present study is an important issue. A theoretical examination of the spin dynamics at finite temperatures in a frustrated system exhibiting a successive phase transition is left for future work. Neutron scattering experiments on a single crystal of CsCrF_4 will provide further insights into the spin dynamics. This represents another avenue for future research.

ACKNOWLEDGMENTS

We are grateful to D. Kawana, T. Asami, and R. Sugiura for supporting us during the neutron scattering experiments at HRC and HER. The neutron experiment using the HRC spectrometer at the Materials and Life Science Experimental Facility of J-PARC was performed under a user program (Proposal No. 2019S01). The neutron experiment using HER at JRR-3 was carried out by the joint research at the Institute for Solid State Physics, University of Tokyo (Proposal No. 21403). H.K. was supported by the Support for Pioneering Research Initiated by Next Generation (SPRING) of the Japan Science and Technology Agency (JST). This project was supported by JSPS KAKENHI Grants No. JP19KK0069, No. JP20K20896, and No. JP21H04441.

APPENDIX: CALCULATED INS SPECTRA FOR SPIN STRUCTURE IN IT PHASE

INS spectra in the IT phase were calculated for two set of parameters, cases A1 and A2, as listed in Table III. Con-

TABLE III. Parameters of the spin Hamiltonian for the calculation of the INS spectra in the IT phase.

	J_0 (meV)	J_1 (meV)	J_2 (μeV)	d_1 (μeV)	D (μeV)
Case A1	2.55 (5)	1.10 (5)	-7 (1)	-51 (1)	0
Case A2	2.39 (5)	1.02 (5)	-8	-55 (1)	-4.6

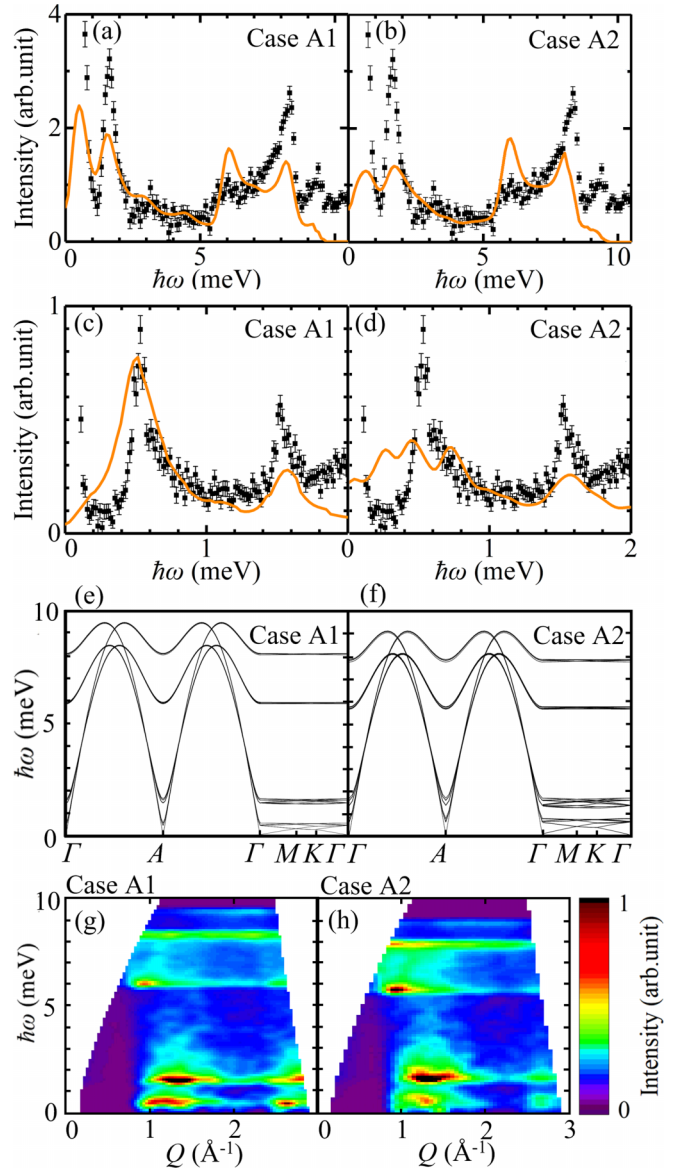


FIG. 7. Calculated INS spectra in the IT phase. (a)–(d) One-dimensional cuts of calculated INS spectra (orange curves) using the spin parameters summarized in Table III and those from experiment (symbols) measured at 3.1 K in the IT phase. The spectra for case A1 in (a) wide and (c) narrow energy ranges. The spectra for case A2 in (b) wide and (d) narrow energy ranges. Calculated dispersion curves for (e) case A1 and (f) case A2. Calculated powder-averaged spectra for (g) case A1 and (h) case A2.

ventional linear spin wave (LSW) theory was used as in the calculation in the LT phase. The $\sqrt{3} \times \sqrt{3}$ structure shown in Fig. 1, which is the ground state of the spin Hamiltonian with the parameters, was used. It is one of the magnetic structures previously proposed [15]. Another one is the 120° structure with spin modulation. It is not the ground state of the spin Hamiltonian, and LSW theory cannot be applied. The temperature was assumed to be 0 K. In Ref. [15], the estimated moment for the LT phase was $1.50\mu_B$, and the one for the $\sqrt{3} \times \sqrt{3}$ structure in the IT phase was $1.62\mu_B$. In the LSW calculation, a change in the magnetic moment simply

changes the scale factor of the dynamical structure factor of the neutron while keeping its profile the same. Thus, a full moment of spin $S = 3/2$ of $3\mu_B$ for a gyromagnetic ratio of 2 was used for both the LT and IT phases for simplicity. The spin correlation was assumed to be long range, even though a short-range correlation was reported [15].

In case A1, D was fixed to zero, and J_0 , J_1 , J_2 , and d_1 were determined so that the calculated energy of the excitations in the IT phase in 1D cuts coincided with the observed one, as determined in LT phase. In case A2, J_2 was fixed to $-8 \mu\text{eV}$, and D was fixed to $-4.6 \mu\text{eV}$; other parameters were determined using the same method as for case A1. The calculated 1D cuts using the best parameters in case A1 in Table III are shown by orange curves in Figs. 7(a) and 7(c) for wide and narrow energy ranges, respectively. The excitation with a peak energy of 0.5 meV can be produced by J_2 instead of D ; however, the peak width is wider than the

energy resolution in Fig. 7(c). The intensities of the peaks, particularly at 6 and 8 meV, in Fig. 7(a) are not reproduced. The calculated 1D cuts using the best parameters in case A2 in Table III are shown by orange curves in Figs. 7(b) and 7(d) for wide and narrow energy ranges, respectively. The low-energy mode at $\hbar\omega \sim 0.5$ meV is lifted by both D and J_2 , leading to a complex profile. Calculated dispersion curves among reciprocal lattice points with high symmetry are shown in Fig. 7(e) for case A1 and Fig. 7(f) for case A2. The calculated spectra after powder averaging are shown in Fig. 7(g) for case A1 and Fig. 7(h) for case A2. Gapless modes stemming from point A in Figs. 7(e) and 7(f) induce finite intensities below 0.5 meV in Figs. 7(g) and 7(h), which contradicts the experiment. The measured spectrum is thus not reproduced by the calculation. The change in the parameters leads to a drastic change in the INS spectrum, even though the change is small.

-
- [1] R. Moessner and S. L. Sondhi, *Phys. Rev. B* **63**, 224401 (2001).
 [2] K. Kawano and M. Takahashi, *J. Phys. Soc. Jpn.* **66**, 4001 (1997).
 [3] H.-T. Wang, *Phys. Rev. B* **64**, 174410 (2001).
 [4] A. Lüscher, R. M. Noack, G. Misguich, V. N. Kotov, and F. Mila, *Phys. Rev. B* **70**, 060405(R) (2004).
 [5] S. Nishimoto and M. Arikawa, *Phys. Rev. B* **78**, 054421 (2008).
 [6] H. J. Schmidt and J. Richter, *J. Phys. A* **43**, 405205 (2010).
 [7] S. Nishimoto, Y. Fuji, and Y. Ohta, *Phys. Rev. B* **83**, 224425 (2011).
 [8] M. Lajko, P. Sindzingre, and K. Penc, *Phys. Rev. Lett.* **108**, 017205 (2012).
 [9] T. Sakai, M. Sato, K. Okunishi, Y. Otsuka, K. Okamoto, and C. Itoi, *Phys. Rev. B* **78**, 184415 (2008).
 [10] M. Sato, *Phys. Rev. B* **75**, 174407 (2007).
 [11] H. Manaka, Y. Hirai, Y. Hachigo, M. Mitsunaga, M. Ito, and N. Terada, *J. Phys. Soc. Jpn.* **78**, 093701 (2009).
 [12] H. Manaka, T. Etoh, Y. Honda, N. Iwashita, K. Ogata, N. Terada, T. Hisamatsu, M. Ito, Y. Narumi, A. Kondo, K. Kindo, and Y. Miura, *J. Phys. Soc. Jpn.* **80**, 084714 (2011).
 [13] H. Manaka and Y. Miura, *J. Korean Phys. Soc.* **62**, 2032 (2013).
 [14] H. Manaka, H. Morita, T. Akasaka, Y. Miura, M. Hagihala, S. Hayashida, M. Soda, and T. Masuda, *J. Phys. Soc. Jpn.* **88**, 114703 (2019).
 [15] M. Hagihala, S. Hayashida, M. Avdeev, H. Manaka, H. Kikuchi, and T. Masuda, *npj Quantum Mater.* **4**, 14 (2019).
 [16] S. Hayashida, M. Hagihala, M. Avdeev, Y. Miura, H. Manaka, and T. Masuda, *Phys. Rev. B* **102**, 174440 (2020).
 [17] J. Villain, R. Bidaux, J.-P. Carton, and R. Conte, *J. Phys. (Paris)* **41**, 1263 (1980).
 [18] A. Chubukov, *Phys. Rev. Lett.* **69**, 832 (1992).
 [19] S. Sachdev, *Phys. Rev. B* **45**, 12377 (1992).
 [20] T. Inami, M. Nishiyama, S. Maegawa, and Y. Oka, *Phys. Rev. B* **61**, 12181 (2000).
 [21] A. S. Wills, *Phys. Rev. B* **63**, 064430 (2001).
 [22] A. S. Wills, A. Harrison, C. Ritter, and R. I. Smith, *Phys. Rev. B* **61**, 6156 (2000).
 [23] D. Grohol, D. G. Nocera, and D. Papoutsakis, *Phys. Rev. B* **67**, 064401 (2003).
 [24] T. Inami, T. Morimoto, M. Nishiyama, S. Maegawa, Y. Oka, and H. Okumura, *Phys. Rev. B* **64**, 054421 (2001).
 [25] T. Nagamiya, S. Tomiyoshi, and Y. Yamaguchi, *Solid State Commun.* **42**, 385 (1982).
 [26] S. Hayashida, H. Ishikawa, Y. Okamoto, T. Okubo, Z. Hiroi, M. Avdeev, P. Manuel, M. Hagihala, M. Soda, and T. Masuda, *Phys. Rev. B* **97**, 054411 (2018).
 [27] S. Hayashida, H. Ishikawa, Y. Okamoto, T. Okubo, Z. Hiroi, G. J. Nilsen, H. Mutka, and T. Masuda, *Phys. Rev. B* **101**, 214409 (2020).
 [28] J.-C. Domenge, P. Sindzingre, C. Lhuillier, and L. Pierre, *Phys. Rev. B* **72**, 024433 (2005).
 [29] H. Ishikawa, T. Okubo, Y. Okamoto, and Z. Hiroi, *J. Phys. Soc. Jpn.* **83**, 043703 (2014).
 [30] K. Seki and K. Okunishi, *Phys. Rev. B* **91**, 224403 (2015).
 [31] S. Itoh, T. Yokoo, S. Satoh, S. Yano, D. Kawana, J. Suzuki, and T. J. Sato, *Nucl. Instrum. Methods Phys. Res., Sect. A* **631**, 90 (2011).
 [32] D. Kawana, M. Soda, M. Yoshida, Y. Ikeda, T. Asami, R. Sugiura, H. Yoshizawa, T. Masuda, T. Hawaii, S. Ibuka, T. Yokoo, and S. Itoh, *J. Phys.: Conf. Ser.* **1021**, 012014 (2018).
 [33] A. K. Freund, *Nucl. Instrum. Methods Phys. Res., Sect. A* **242**, 28 (1985).
 [34] R. Vorderwisch, U. Stuhr, and S. Hautecler, *J. Neutron Res.* **7**, 119 (1999).
 [35] S. Toth and B. Lake, *J. Phys.: Condens. Matter* **27**, 166002 (2015).
 [36] A. J. Dianoux and G. H. Lander, *Neutron Data Booklet* (Old City Publishing, Philadelphia, USA, 2003).
 [37] H.-J. Koo, *J. Magn. Magn. Mater.* **324**, 2806 (2012).
 [38] A. B. Harris, C. Kallin, and A. J. Berlinsky, *Phys. Rev. B* **45**, 2899 (1992).
 [39] M. Maksymenko, R. Moessner, and K. Shtengel, *Phys. Rev. B* **96**, 134411 (2017).
 [40] K. Matan, D. Grohol, D. G. Nocera, T. Yildirim, A. B. Harris, S. H. Lee, S. E. Nagler, and Y. S. Lee, *Phys. Rev. Lett.* **96**, 247201 (2006).
 [41] M. Maksymenko, V. R. Chandra, and R. Moessner, *Phys. Rev. B* **91**, 184407 (2015).

- [42] J. M. Luttinger and L. Tisza, *Phys. Rev.* **70**, 954 (1946).
- [43] D. Litvin, *Physica (Amsterdam)* **77**, 205 (1974).
- [44] T. B. S. Jensen, N. B. Christensen, M. Kenzelmann, H. M. Rønnow, C. Niedermayer, N. H. Andersen, K. Lefmann, M. Jiménez-Ruiz, F. Demmel, J. Li, J. L. Zarestky, and D. Vaknin, *Phys. Rev. B* **79**, 092413 (2009).
- [45] K. M. Ranjith, R. Nath, M. Majumder, D. Kasinathan, M. Skoulatos, L. Keller, Y. Skourski, M. Baenitz, and A. A. Tsirlin, *Phys. Rev. B* **94**, 014415 (2016).
- [46] J. P. Goff, D. A. Tennant, and S. E. Nagler, *Phys. Rev. B* **52**, 15992 (1995).
- [47] M. Mekata, N. Yaguchi, T. Takagi, T. Sugino, S. Mitsuda, H. Yoshizawa, N. Hosoi, and T. Shinjo, *J. Phys. Soc. Jpn.* **62**, 4474 (1993).
- [48] S. Mitsuda, N. Kasahara, T. Uno, and M. Mase, *J. Phys. Soc. Jpn.* **67**, 4026 (1998).
- [49] A. Harrison, M. F. Collins, J. Abu-Dayyeh, and C. V. Stager, *Phys. Rev. B* **43**, 679 (1991).
- [50] W. J. L. Buyers, R. M. Morra, R. L. Armstrong, M. J. Hogan, P. Gerlach, and K. Hirakawa, *Phys. Rev. Lett.* **56**, 371 (1986).
- [51] M. C. Martin, M. Hase, K. Hirota, G. Shirane, Y. Sasago, N. Koide, and K. Uchinokura, *Phys. Rev. B* **56**, 3173 (1997).
- [52] Y. Uchiyama, Y. Sasago, I. Tsukada, K. Uchinokura, A. Zheludev, T. Hayashi, N. Miura, and P. Böni, *Phys. Rev. Lett.* **83**, 632 (1999).
- [53] A. Zheludev, T. Masuda, I. Tsukada, Y. Uchiyama, K. Uchinokura, P. Böni, and S.-H. Lee, *Phys. Rev. B* **62**, 8921 (2000).